Int J Adv Manuf Technol
DOI 10.1007/s00170-015-7729-3

ORIGINAL ARTICLE

Experimental evaluation on mechanical properties of a riveted structure with electromagnetic riveting

Xu Zhang[1] · **Hai Ping Yu**[1,2] · **Hai Su**[3] · **Chun Feng Li**[1,2]

Received: 29 May 2015 / Accepted: 17 August 2015

Abstract Evaluation on mechanical properties of a riveted structure with electromagnetic riveting was performed experimentally in this work. The effect of rivet tail dimension on mechanical properties and microstructure evolution were investigated by controlling deformation. The possibility of substituting a riveted structure for a bolted structure was explored by the contrast analysis. Results showed that dislocation slip in the adiabatic shear band was a main deformation mechanism of rivet tail. The rivet tail dimension mainly determined pull-out strength and failure mode of the riveted structure, and the optimal height of rivet tail was 5~6 mm for this riveted structure. The maximum bearing loads of shear tests and pull-out tests were 23.3 and 35.0 kN, respectively. Both shear strength and pull-out strength of riveted structures exceeded that of bolted structures, where the bolt has similar tensile-loading capacity as the rivet shaft. In contrast to the bolted structure, the load-to-weight ratio values of the riveted structure for shear test and pull-out test were improved by 22.64 and 66.10 %, respectively.

Keywords Electromagnetic riveting · Experimental evaluation · Microstructure · Mechanical properties

✉ Hai Ping Yu
haipingy@hit.edu.cn

[1] School of Materials Science and Engineering, Harbin Institute of Technology, Harbin 150001, China

[2] National Key Laboratory for Precision Hot Processing of Metals, Harbin Institute of Technology, Harbin 150001, China

[3] Tianjin Long March Launch Vehicle Manufacturing Co. Ltd., Tianjin, China

1 Introduction

In the aerospace manufacturing industry, it is difficult to realize the integral forming of large components using traditional techniques. Consequently, many aircrafts consist of a large sum of manufacturing parts attained by different processing technologies. Mechanical joining techniques have been inevitably used in an assembly process [1]. Mechanical joining technique mainly includes welding, bolting, and riveting [2]. Among them, weld cracking usually occurs due to stress concentration in the welding joints. And the looseness in the bolting joints greatly reduces the connection reliability. The riveting process has, by contrast, some characteristics of simple process, reliable connection quality, and good seal [3, 4]. So the riveting process has been widely used in aerospace field, especially in connections between aircraft's covering skin and framework. In addition, some materials (such as titanium alloy rivets and composites) will be widely used in aerospace manufacturing fields so as to reduce weight. These materials have lower density, higher strength, and higher corrosion resistance, causing that traditional riveting technique (usually for the pneumatic riveting process in the aerospace field) will face some new challenges. Composite sheets are prone to damage under the extruding effect of rivets during the riveting process. Titanium alloy rivets have the great deformation resistance at room temperature and is difficult to be formed with the pneumatic riveting.

Electromagnetic forming (EMF) [5] is a high-speed forming technology and has been applied to joining processes [6], powder compaction [7], and formations of sheets [8–10]. As a method of the EMF process, the electromagnetic riveting (EMR) has some advantages, such as the high-speed loading, the larger impact force, and the deformation stability. So the uniform interference can

Published online: 27 August 2015

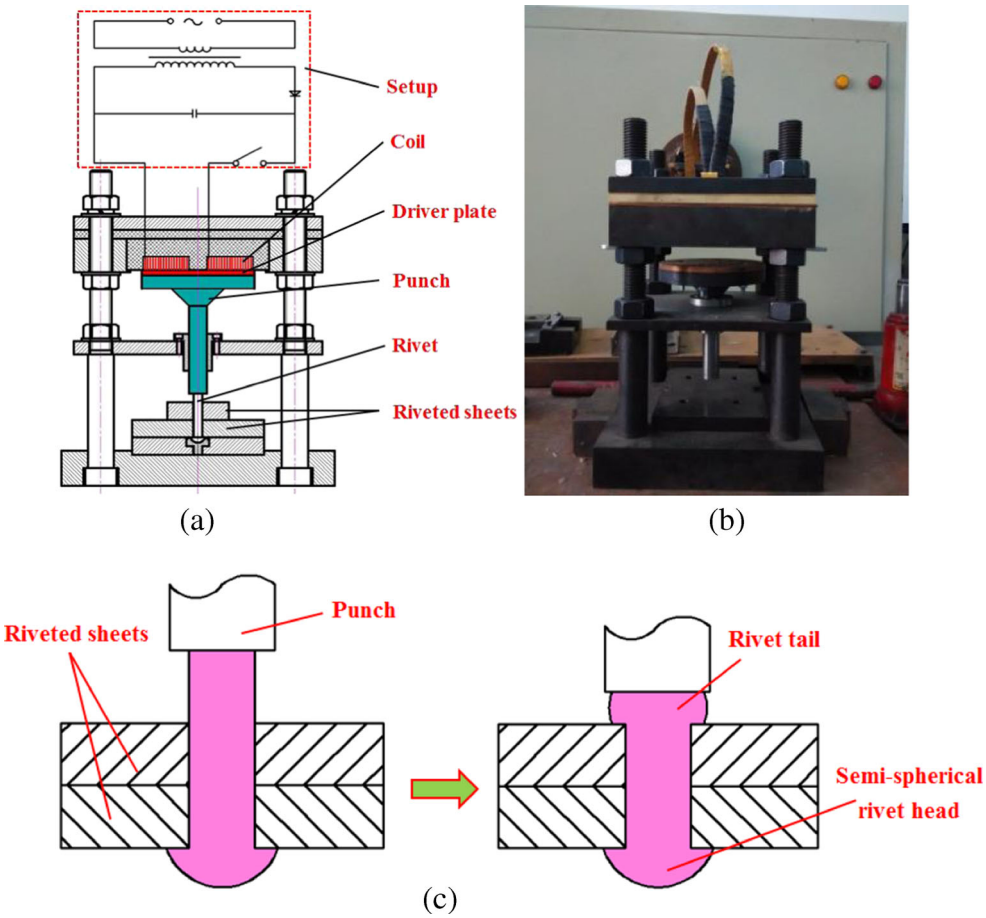

Fig. 1 Schematic and setup of the electromagnetic riveting process: **a** the EMR schematic, **b** the experimental mold, and **c** the formation process

facilitate applications in composite material components with the riveted joint. In addition, difficult deformation of titanium alloy rivets can be overcome under adequate riveting forces. Based on these advantages, numerous researchers have employed experimental investigations into this process. Choo et al. [11] reported that the high strain rate induced the precipitation hardening in adiabatic shear bands and led to the failure of 7075-T73 aluminum rivets. Investigations by Deng et al. [12] showed that the deformation mechanism of EMR was the adiabatic shearing deformation and dynamic recrystallization in adiabatic shear bands (ASBs) of TA1 titanium alloy rivets. The FE simulation by Zhang [13] demonstrated the strain highly concentrated in ASBs and the maximum temperature rise reached to 500 °C. In addition, mechanical properties (shear strength and pull-out strength) of riveted structures are important evaluation indexes of riveting qualities. Feng et al. [14] showed that both shear strength and pull-out strength of the EMR-riveted structures were significantly higher than that of the pneumatic riveting. Currently, some load-bearing structures of a spacecraft are generally joined with Φ6 mm-30CrMnSi bolts. However, strength-to-weight ratio and the reliability of bolted structures are relatively lower. In order to reduce spacecraft weight, riveted structures with high strength-to-weight ratio aluminum alloys might be applied to substitute bolted structures. But small size rivets are unable to meet the strength requirement. And the riveting capacity of the conventional pneumatic riveting is only suitable for aluminum alloy rivets with the diameter of less than or equal

Table 1 The parameters of an electromagnetic forming machine

Equipment type	Maximum energy (kJ)	Discharge voltage (V)	Discharge capacitance (μF)
EMF30/5-IV	33.6	0~5000	192 μF×14

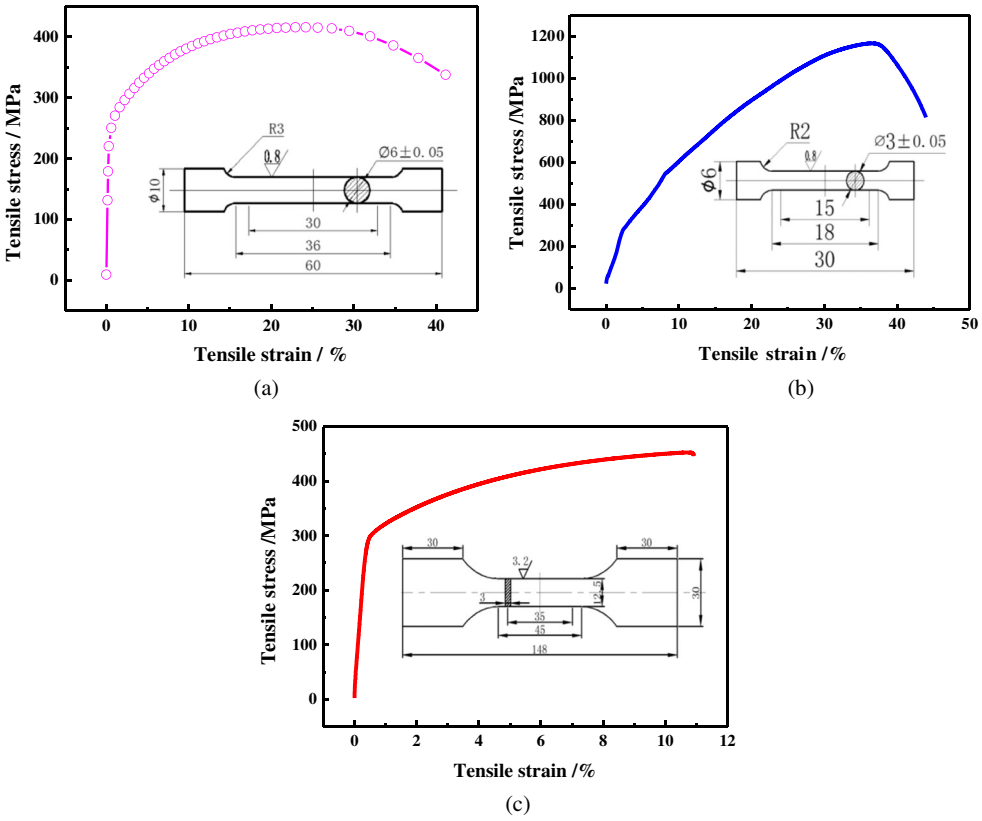

Fig. 2 Stress-strain curves under quasi-static tensile tests: **a** 2A10 aluminum alloy rivets, **b** 30CrMnSi bolts, and **c** 2A12-T4 aluminum alloy sheets

to 6 mm. Consequently, the new riveting technique is needed to form larger rivets which are able to compete with Φ6 mm-30CrMnSi bolts. The EMR technique with many advantages can be competent to form larger-size rivets. However, present investigations rarely focused on the quality of EMR with larger-size rivets and lightweight strategy of substituting a bolted structure with a riveted structure.

In this work, Φ10 mm-2A10 aluminum alloy rivets were used in EMR experiments. Microstructure observation in the rivet tail and the effect of the rivet tail dimension on mechanical properties of riveted structures were investigated to determine the optimal dimension of the rivet tail. Mechanical properties of riveted structures were tested and evaluated experimentally. Furthermore,

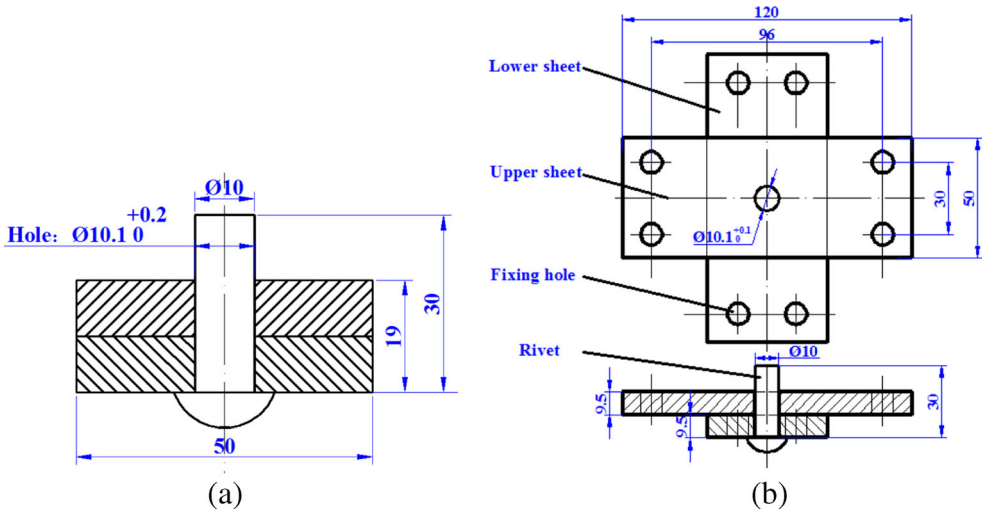

Fig. 3 The sketch of riveted specimen preparation: **a** the macro dimension and microstructure observation specimen and **b** mechanical property test specimen

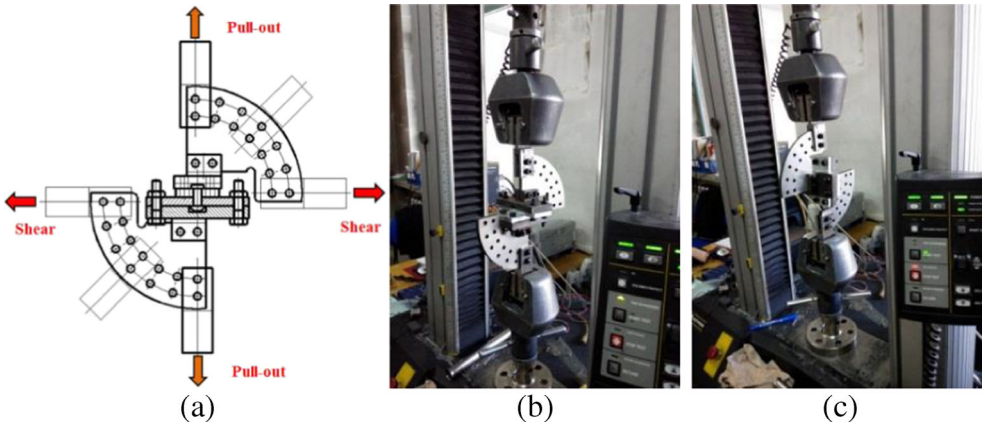

Fig. 4 The schematic of multifunction fixing setup and testing process: **a** the fixing setup schematic, **b** a pull-out test, and **c** a shear test

the possibility of substituting a bolted structure with a riveted structure was explored.

2 Experimental materials and method

2.1 The electromagnetic riveting process

The principle of the electromagnetic riveting process is shown in Fig. 1. Capacitors in the setup (Fig. 1a) get charged to a certain voltage. During the discharge process, the high-amplitude alternating current runs through the flat spiral coil embedded in the mold (Fig. 1b). And then an induced eddy current generates in the driver plate (a pure copper plate with the high conductivity). The two opposing currents cause induced magnetic fields, respectively. Consequently, forces acted on the punch originate from the repulsive force between the two magnetic fields. In addition, the EMR process can give rise to a strain rate of 10^3 s^{-1} [15]. Figure 1c shows that the rivet shaft is upset to form the rivet tail during the EMR process. The formation of the rivet tail is similar to other riveting processes and is used to lock the two sheets [16].

EMR experiments were carried out by an EMF30/5-IV electromagnetic forming (EMF) machine at Harbin Institute of Technology. Parameters of the EMF machine are shown in Table 1. Because this machine has 14 capacitors and the adjustable range of the capacitance is limited, the capacitance was set to 1536 μF (eight capacitors) in this work. And deformations of rivets were controlled by adjusting discharge voltages.

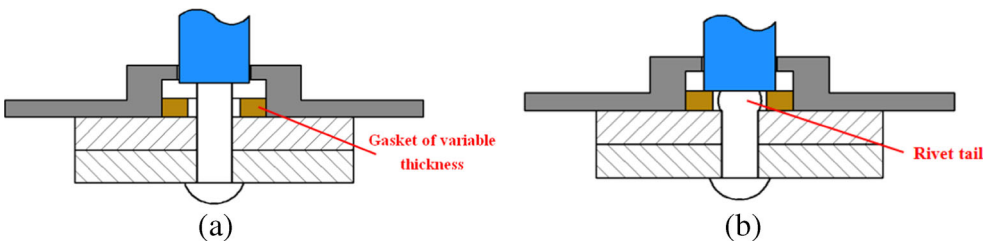

Fig. 5 Schematic of the setup using to control deformation: **a** the state before deformation and **b** the state after deformation

2.2 Rivet materials and sample preparation

The as-received rivet with semi-spherical rivet head was 2A10 aluminum alloy, which was the quench aging alloy with a chemical composition (wt%) of 0.25 Si, 0.20 Fe, 3.9–4.5 Cu, 0.30–0.50 Mn, 0.15–0.30 Mg, 0.10 Zn, 0.15 Ti, and balance Al. Microstructures of original rivets were uniform equiaxial grains with the diameter of 50 μm. And the riveted sheets were 2A12-T4 aluminum alloy. In addition, the bolt used for the contrast analysis was a 30CrMnSi alloy steel. Their tensile property curves were obtained using the Instron 5569 tensile testing machine with a 2 mm/min velocity, as shown in Fig. 2. Tensile testing specimens of rivets were cut from shaft of Φ10 mm×60 mm rivets and were manufactured according to the standard requirement.

30CrMnSi bolts (including a screw nut, a spring washer, and a flat washer) were used for bolted structures. The size of a bolt was determined as Φ6 mm×30 mm, which has been usually used for joining structures in the aerospace. Figure 2b shows that the tensile strength of the bolt is 1166 MPa. In general, the material shear strength is about 0.6 times greater than the tensile strength. Consequently, it is calculated with the Eq. (1) that the maximum bearable shear load (MBSL) is 19.8 kN along the radial direction:

$$F_{\mathrm{Max}} = \sigma_\tau \frac{\pi}{4} d^2 \tag{1}$$

where σ_τ represents shear strength, and d is the diameter of a rivet shaft. In order to reduce weight and improve the joining

Fig. 6 Mechanical property samples after the EMR process

reliability without losing carrying capacity, it is meaningful and interesting to explore the possibility to substitute a bolted structure with a riveted structure, namely to use equivalent or higher strength rivets as substitutes for bolts. However, the

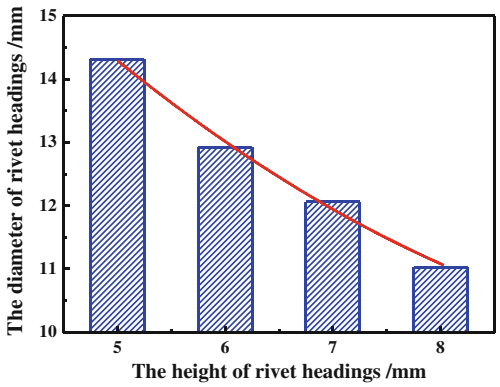

Fig. 7 The diameters of rivet tails under varying heights

MNSL of a Φ10 mm-2A10 aluminum alloy rivet is calculated to be 19.5 kN through the tensile strength shown in Fig. 2a. This MNSL just satisfies with the equivalent strength requirement. Facilitating the contrastive analysis between riveted structures and bolted structures, the thickness of dual-layers sheets for bolted structures is identical to that of riveted structures. The sketch of riveted specimens is demonstrated in Fig. 3. And the size of a rivet was selected as Φ10 mm× 30 mm. The riveted sheets were mechanically processed into 9.5-mm thickness sheets with prefabricated holes in the center of them. In order to ensure the accuracy (Φ10.1~10.2 mm) of the diameter of a prefabricated hole, the hole was prepared by a CNC electrical discharge machine. In addition, the whole riveted structure included two layers sheets with a rivet and the length of the rivet shaft outsides sheets was 11 mm before the EMR deformation.

2.3 Mechanical property measuring method

Mechanical property tests of riveted structures and bolted structures were performed with an Instron 5569 universal testing machine. All mechanical property tests were employed with a 5 mm/min tensile velocity. The schematic of a multifunction fixing setup is presented in Fig. 4a. The fixing setup is suitable for mechanical property tests with different loading directions. The shear tests were done under the loading direction perpendicular to the axis of a rivet. And the pull-out tests were executed under the loading direction parallel to the axis of a rivet. Specimens in this work were tested under two loading conditions (pull-out loading and shear loading), as shown

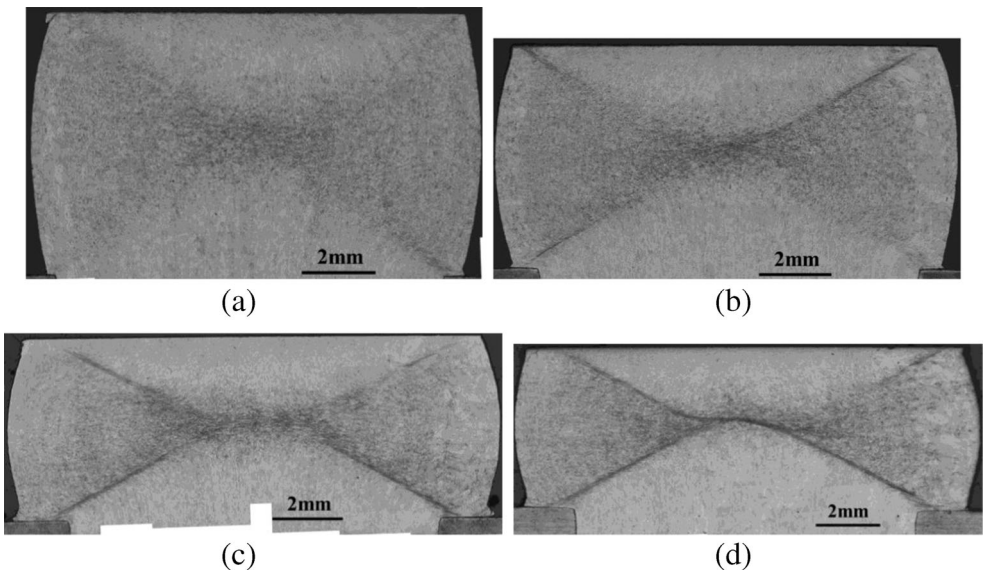

Fig. 8 Microstructure observation in rivet tails: **a** ε= 27.3 %, **b** ε=36.4 %, **c** ε=45.5 %, and **d** ε=54.5 %

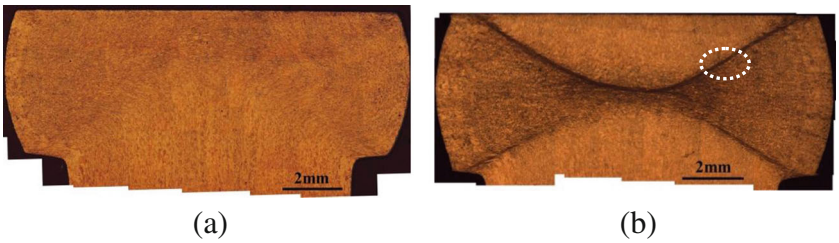

Fig. 9 Contrast analysis of microstructures in rivet tails: **a** the conventional pressure riveting and **b** the electromagnetic riveting

in Fig. 4b, c. The load-displacement curves were recorded by the tensile tester.

2.4 Controlling method of the rivet tail dimension

During a riveting process, the rivet deformation refers primarily to the upsetting process of rivet tail. So the formation of rivet tail directly determines mechanical properties of riveted structures. In order to investigate the effect of rivet tail dimension on mechanical properties of riveted structures, the load-displacement curves of shear tests and pull-out tests were obtained for riveted structures with different heights of rivet tails. A setup for controlling method of rivet tail dimension is shown in Fig. 5. The axial deformation of rivet tail is controlled by adjusting the thickness of rigid gasket during the EMR process. The height of rivet tail should be generally controlled within the universal riveting requirement (4 mm in minimum height). Mechanical properties of riveted structures under varying heights (5, 6, 7, and 8 mm) of rivet tails were investigated. And all the mechanical property samples were prepared with the relatively higher discharge 2.6 kV.

Four groups with different thickness gaskets (5, 6, 7, and 8 mm) were used to conduct EMR experiments under the discharge voltage 2.6 kV. Mechanical property samples after the EMR process are shown in Fig. 6. And measured results of rivet tail dimensions are presented in Fig. 7. According to the constant volume during the plastic deformation, the diameter of rivet tail increased as the height of that reduced.

In order to explore the formation process and microstructural quality of rivet tail before mechanical property

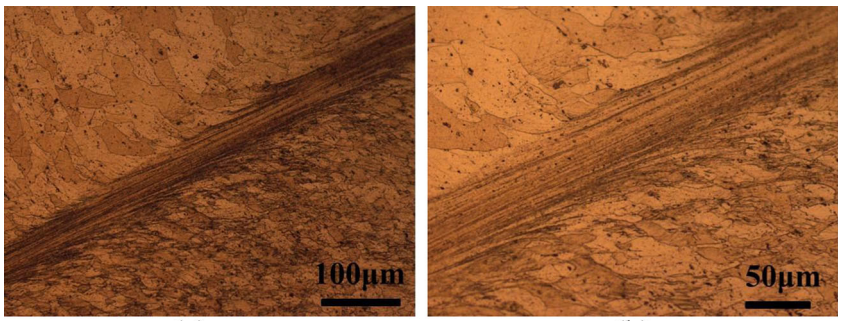

Fig. 10 An adiabatic shear band in rivet tail of electromagnetic riveting: **a** the morphology of the ASB and **b** the partial enlarged drawing

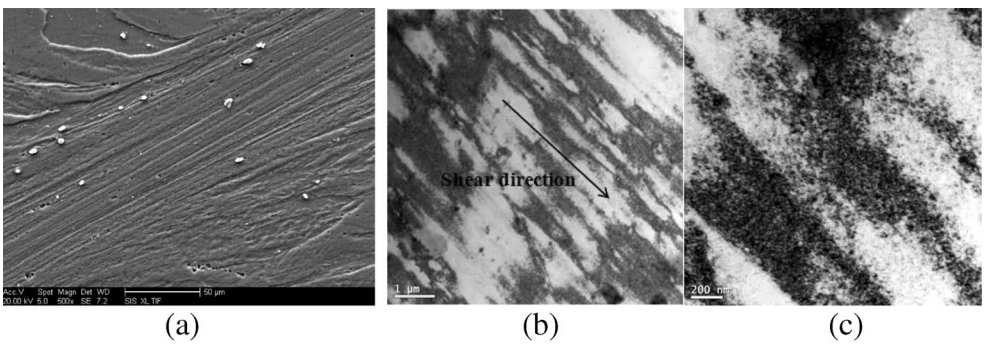

Fig. 11 Microstructure observation of the adiabatic shear band (ASB) in the rivet tail: **a** the SEM morphology of the ASB, **b** the TEM microstructure in the ASB, and **c** dislocations tangle

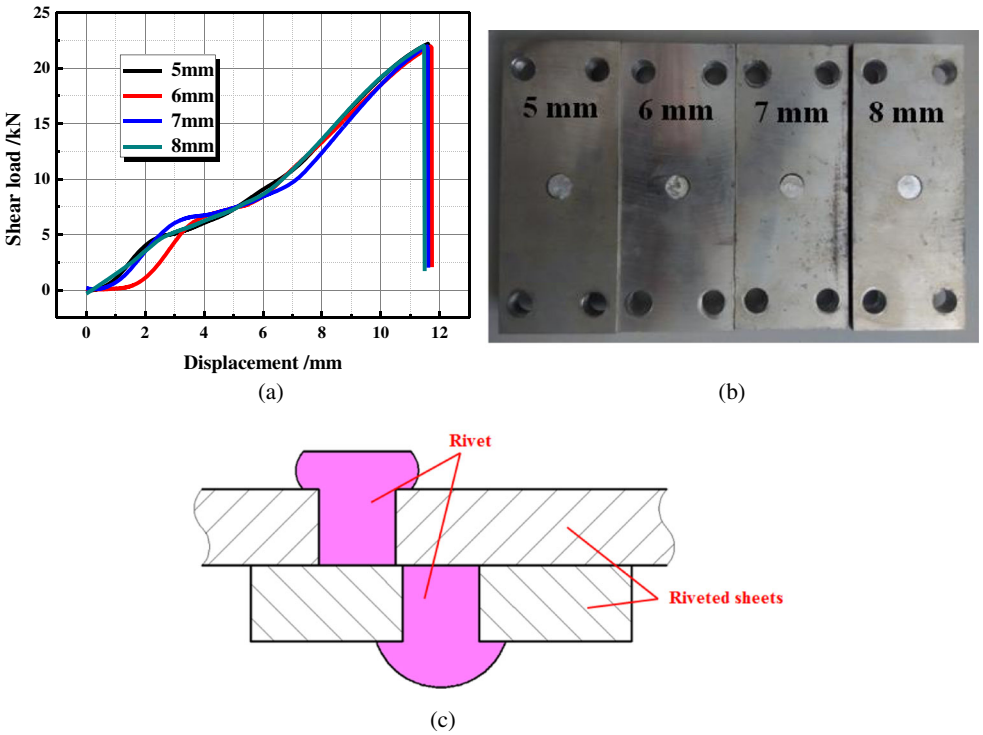

Fig. 12 The shear load-displacement curves and rupture samples of riveted structures with different rivet tail heights: **a** load-displacement curves, **b** rupture samples, and **c** the rupture mode

tests, the deformation process with a certain discharge voltage can be discretized to some stages. And the microstructure and dimension of rivet tail in each stage is observed to reveal the whole process. However, the setup (Fig. 5) of deformation control can make the process possible. The deformation of rivet tail for every stage is controlled by adjusting the thickness of rigid gasket during EMR process. In addition, the EMR experiment for every stage was carried out with same discharge parameters. Thus, results of different stages can be approximately considered as the results at different moments of the continuous process. The section of specimens obtained by the spark-erosion wire was mechanically polished and etched with the Keller's reagent (95 %—H_2O, 2.5 %—HNO_3, 1.5 %—HCl, and 1.0 %—HF). And then corrosion products on the surface of etched specimens were removed with a solution of 10 ml—HNO_3 and 40 ml—H_2O. Metallographic characterization was performed by a Zeiss optical microscopy. Microstructure observation in the section of rivet tail is shown in Fig. 8. These figures were montaged with many metallographs. The adiabatic shear bands (ASBs) existed in the rivet tails. The engineering strain along the height of rivet tail can be calculated using the equation ($\varepsilon=(h_0-h)/h_0$), where h represents the height after deformation and h_0 represents the length of rivet shaft outsides sheets. Two shear bands initiated in the diagonal direction as strain added up to 27.3 %. In addition, the deformation in the center got more severe. The shear deformation concentration began at diagonal points and gradually spread to the central as strain continued to accumulate and encountered in the central. In conclusion, it can be illustrated that the formation of an adiabatic shear band was influenced by the strain accumulation. Although the deformation distribution within the rivet tail was inhomogeneous due to shear deformation concentration, no cracks occurred in microstructures.

3 Results and discussion

3.1 Microstructure evolution in the rivet tail

ASB was an important phenomenon under the high strain rate deformation. The ASB phenomenon is a

Table 2 The diameters of deformed rivet shafts in the contact plane between dual-layers sheets

The height of rivet tail (mm)	Diameters of rivets after EMR (d) (mm)
5	10.26
6	10.26
7	10.16
8	10.20

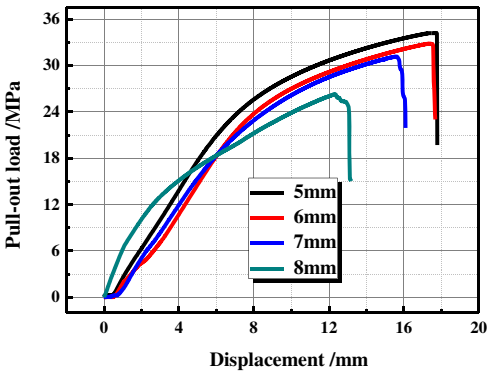

(a)

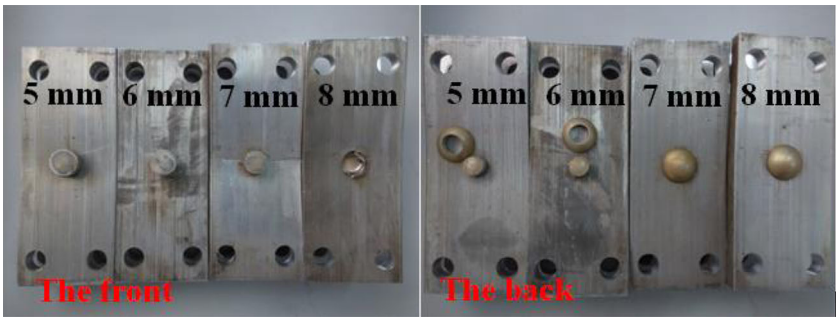

(b)

Fig. 13 The pull-out load-displacement curves and rupture samples of riveted structures with different rivet tail heights: **a** load-displacement curves and **b** rupture samples

distinctive feature of the shear deformation concentration. However, the electromagnetic riveting is one of high-speed formations, in which the strain rate is the higher than 10^3 s^{-1}. Figure 9 demonstrates that contrast results in rivet tails between a conventional pressure riveting and an electromagnetic riveting. The loading velocity of the pressure riveting was 2 mm/min. The shape of the rivet tail for the conventional pressure riveting (Fig. 9a) was similar to that of electromagnetic riveting. But the distribution uniformity of microstructures in rivet tail was superior to that of the electromagnetic riveting, and the high deformation concentration did not occur. Figure 10 shows that the morphology of the ASB which is selected in the white marked zone of the Fig. 9b. It can be seen in Fig. 10 that the microstructure in the ASB was remarkably distinct from that of other parts. Most plastic deformation highly concentrated in the ASB from the grain appearance. The grains in the ASB were significantly elongated and distorted along deformation streamlines, indicating that the metal had severe shearing plastic deformation. Moreover, microstructures in the ASB presented the morphology of fiber structures. The ASB drove the deformation of metals near them, and these metals flew

Table 3 Maximum load results for shear tests and pull-out tests

The height of rivet tail (mm)	Maximum shear load (kN)	Maximum pull-out load (kN)
5	21.9, 22.8, 22.6, 22.5, 22.8	34.6, 34.6, 34.5, 34.2, 34.1
	Average value: 22.5	Average value: 34.4
6	21.9, 21.9, 23.2, 22.3, 22.4	32.8, 32.6, 32.6, 32.4, 32.2
	Average value: 22.3	Average value: 32.5
7	21.9, 22.6, 22.6, 22.4, 22.1	31.3, 31.2, 30.8, 30.6, 30.4
	Average value: 22.3	Average value: 30.9
8	22.1, 22.4, 21.8, 22.2, 22.1	26.8, 26.6, 26.3, 26.1, 25.8
	Average value: 22.1	Average value: 26.2

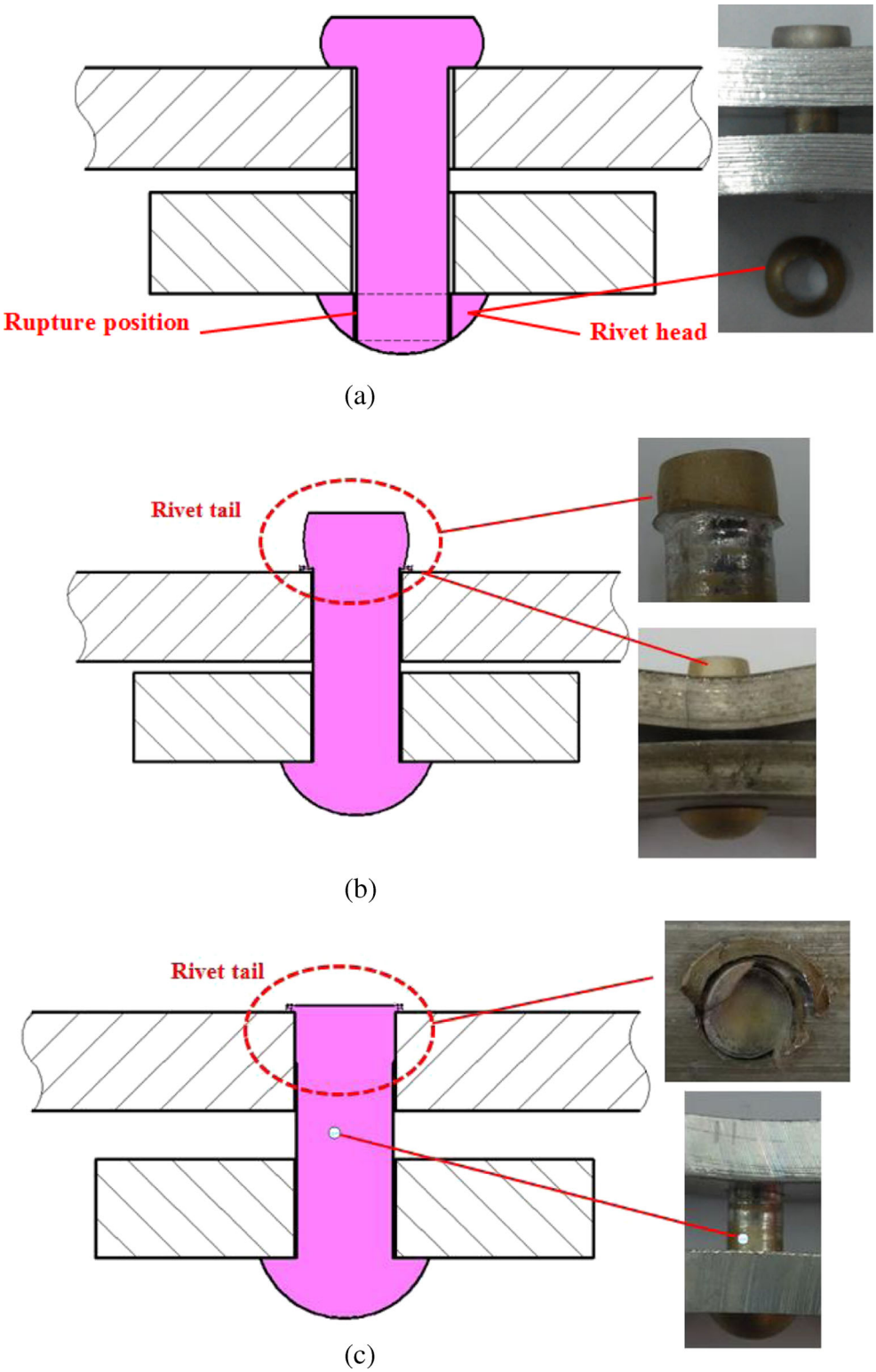

Fig. 14 Rupture modes for pull-out samples with different rivet tail heights: **a** rivet tail with 5 or 6 mm height, **b** rivet tail with 7 mm height, and **c** rivet tail with 8 mm height

into ASBs. So the streamlines of the ASB were not smooth and showed lamellar morphology. The width of ASB were about 50~80 μm.

Figure 11 shows the SEM morphology of an adiabatic shear band and the TEM microstructure in the ASB. The SEM morphology with the greater enlargement indicated that

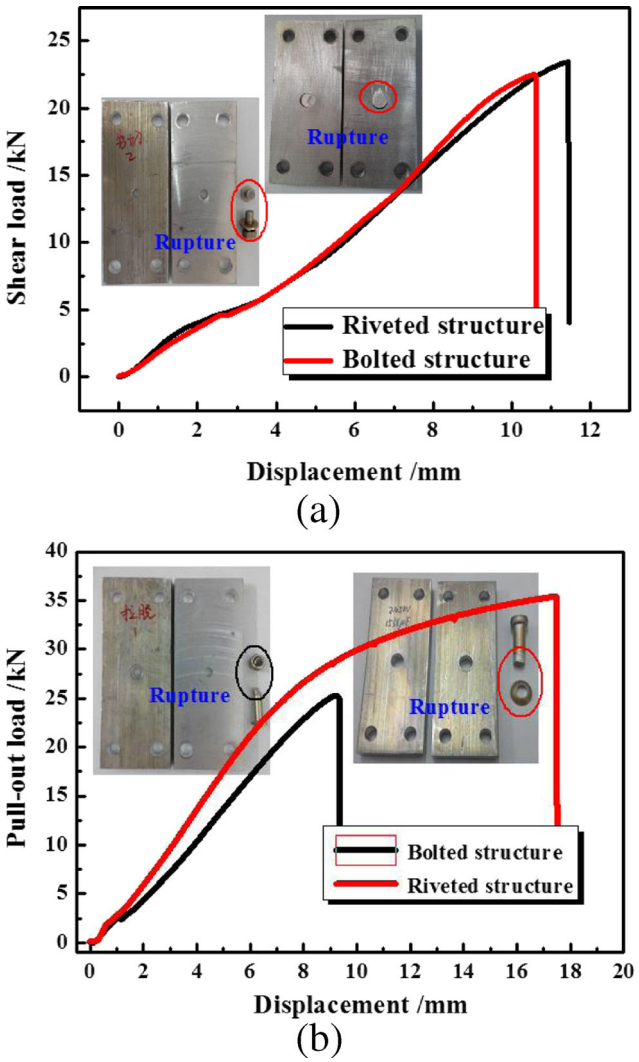

Fig. 15 The typical load-displacement for riveted structures and bolted structures: **a** shear loads and **b** pull-out loads

the fibrous microstructures were relatively straight inside the ASB. However, the microstructures in the outside edges of the ASB were a smooth transition from some greater grains. In addition, many white second-phase particles scattered inside the ASB. Figure 11b, c presents that a high density of dislocations is noticed in the ASB, and the dislocations tangle each other. Elongated dislocation cells are observed along the shear direction in Fig. 10c, demonstrating that the deformation mechanism of the ASB is dislocation slip and severe shear plastic deformation occurred in the ASB.

3.2 The effect of rivet tail dimension on mechanical properties

Figure 12 shows that typical shear load-displacement curves and fracture samples. And multiple sets of repeated shear tests are shown in Table 3. The variation trends and the maximum shear load were very similar for four riveted structures, demonstrating that the effect of the height of rivet tail on shear load was negligible when the height was 8 mm or less than 8 mm. And all rupture positions (as revealed in Fig. 12b, c) occurred on the contact plane between dual-layers sheets. After EMR experiments, the diameters of deformed rivet shaft on the contact plane between dual-layers sheets were measured, as shown in Table 2. The maximum shear load can be, in theory, approximately calculated by the Eq. (2) mentioned above. The four riveting cases have early equal diameter of rivet shaft on the contact plane between dual-layers sheets. Consequently, the capacity of bearing shear loads showed little change. The changing law accorded with the numerical simulation in electromagnetic riveting by Zhang et al. [17]. Namely, rivet deformation mainly included the whole upsetting of rivet shaft and the formation of rivet tail during the EMR process. Once the rivet tail started to form, the rivet shaft would have little deformation. Thus, the diameter of rivet shaft almost remained unchanged from the initial formation of rivet tail to the end of deformation.

Figure 13 shows that typical pull-out load-displacement curves and fracture samples. And multiple sets of repeated pull-out tests are shown in Table 3. The results demonstrated that the maximum pull-out load increased as the increased height of rivet tail. And the pull-out load of rivet tail with 5 mm height was not much different from that of rivet tail with 6 mm height. Failure positions (Fig. 14a) showed that semi-spherical rivet head of the rivet was sheared to fall out for the two cases. But the rivet tail for the 7 mm height were compressed and slightly broken. For the 8 mm height of rivet tail, the rivet tail was crushed and embedded in a hole of the sheet. The lower rivet tail led to the bigger diameter of it, causing much larger area for bearing load during the pull-out

Table 4 The comparison between riveting structures and bolting structures

	Weight (g)	Maximum shear load (kN)	Load-to-weight ratio (shear load)	Maximum pull-out load (kN)	Load-to-weight ratio (pull-out load)
Φ6 mm-30CrMnSi bolted structures	10.59	22.3, 22.4, 22.5, 22.5, 22.8 Average value: 22.5	2.12	24.5, 24.7,25.2, 25.2, 25.4 Average value: 25.0	2.36
Φ10 mm-2A10 riveted structures	8.92	23.0, 23.0, 23.1, 23.3, 23.6 Average value: 23.2	2.60	34.6, 34.8, 34.8, 35.2, 35.5 Average value: 35.0	3.92
Contrast analysis	Reduction by 15.77 %	Increase by 3.11 %	Increase by 22.64 %	Increase by 40 %	Increase by 66.10 %

loading. In addition, the rivet tail for lower height had large deformation, which contributed to the higher strength due to work hardening effect. Consequently, the height of rivet tail determined the failure mode of riveted structures under pull-out loads. And the optimal height of rivet tail was 5~6 mm for the Φ10-2A10 aluminum alloy rivet.

3.3 Mechanical properties of riveted structure and bolted structure

The shear strength and the pull-out strength were two major evaluation indexes of mechanical properties for mechanical joining structures. Mechanical property samples of riveted structures were prepared according to the optimal height of rivet tail mentioned above. Figure 15 shows typical load-displacement curves of riveted structures and bolted structures under different loading directions, including shear load and pull-out load. Because there existed clearances among pins, bolts, and fixing setup, the initial stages of load-displacement curves fluctuated slightly in the pre-tightness state of the fixing setup. After the adjustment stage, the loads started to increase smoothly until ruptures. For the riveted structures, the rivet shafts were ruptured under shear tests. In addition, the shear plane of shear test was vertical to rivet axis and the rupture position located on the contact plane between upper sheet and lower sheet. The semi-spherical rivet head was sheared to fall out under pull-out load. The loading displacement of the pull-out test was significantly larger than that of shear test, showing stretching diameter shrinkage of rivet occurred before pull-out rupture. For the bolted structures, the variation trend of these curves is parallel to that of riveting structures. The bolt was also ruptured on the contact surface between two layers sheet during shear test. Rupture for pull-out test occurred in thread. Moreover, the maximum bearing shear load and the pull-out load of riveted structures were higher than that of bolted structures. And this tendency was more remarkable for pull-out loading.

In order to explore the possibility of substituting a riveted structure for a bolted structure, the comparison results for riveted structures and bolted structures are shown in Table 4. The load-to-weight ratio (LWR) in this work was used to evaluate proportion in weight reduction. This term is similar to strength-to-weight ratio and is the ratio between the maximum bearing load and the material weight. The capacity of bearing shear load for riveted structures increased slightly comparing with bolted structures. And the bearing capacity of pull-out load increased by 40 %. Furthermore, each rivet could lose 15.77 % weight than a set of bolt (including a screw nut, a spring washer, and a flat washer). Moreover, the LWR values were significantly improved by using the riveted structure, especially for the pull-out loading case. Although weight reduction for the single rivet was negligible, the effect of weight loss was very considerable for a spacecraft with thousands of bolts. In addition, the high capacity of bearing load can also reduce the use count of fasteners.

4 Conclusions

- The rivet tail dimension had virtually no effect on the shear strength of a riveted structure after the formation of a rivet tail. But the dimension significantly determined the pull-out strength and failure mode of riveted structures. The optimal height of a rivet tail was 5~6 mm for Φ the 10-2A10 aluminum alloy rivet.
- Adiabatic shearing is a main deformation mechanism of the rivet tail during EMR process. Adiabatic shear bands (ASBs) were an important characteristic of microstructure. The shear deformation concentration began at diagonal point and gradually spread to the central as strain continued to accumulate and encountered in the central. Microstructure evolution was presented as the dislocation slip.
- Compared with Φ6 mm-30CrMnSi bolted structures, Φ10 mm-2A10 riveted structures can not only improve mechanical properties of joining structures but also realize weight reduction. The load-to-weight ratio values for shear tests and pull-out tests were improved by 22.64 and 66.10 %, respectively.

Acknowledgments This paper was financially supported by the National Basic Research Program of China (973 Program) (2011CB012805). The authors would like to take this opportunity to express their sincere appreciation.

References

1. Groche P, Wohletz S, Brenneis M, Pabst C, Resch F (2014) Joining by forming—a review on joint mechanisms, applications and future trends. J Mater Process Technol 214:1972–1994
2. Mori KI, Bayn FL, Micari F, Tekkaya AF (2013) Joining by plastic deformation. Ann CIRP Manuf Technol 62:673–694
3. Chen NJ, Thonnerieux M, Ducloux R, Wan M, Chenot JL (2014) Parametric study of riveted joints. Int J Mater Form 7:65–79
4. Meschut G, Janzen V, Olfermann T (2014) Innovative and highly productive joining technologies for multi-material lightweight car body structures. J Mater Eng Perform 23:1515–1523
5. Psyk V, Tisch D, Kinsey BL, Tekkaya AE, Kleiner M (2011) Electromagnetic forming—a review. J Mater Process Technol 211:787–829
6. Deng JH, Yu HP, Li CF (2009) Numerical and experimental investigation of electromagnetic riveting. Mater Sci Eng A 499:242–247
7. Wu YC, Huang SY, Chang ZH, Tian ZW (2002) The low-voltage electromagnetic compaction of powder materials. J Wuhan Univ Technol 17:39–42

8. Oliveira DA, Worswivk MJ, Finn M, Newmanc D (2005) Electromagnetic forming of aluminum alloy sheet: free-form and cavity fill experiments and model. J Mater Process Technol 170: 350–362
9. Xu JR, Cui JJ, Lin QQ, Li CF (2014) Effects of driver sheet on magnetic pulse forming of AZ31 magnesium alloy sheets. Int J Adv Manuf Technol 72:791–800
10. Xu JR, Yu HP, Li CF (2013) Effects of process parameters on electromagnetic forming of AZ31 magnesium alloy sheets at room temperature. Int J Adv Manuf Technol 66:1591–1602
11. Choo V, Reinhal PG, Ghassaei S (1989) Effect of high rate deformation induced precipitation hardening on the failure of aluminum rivets. J Mater Sci 24:59–60
12. Deng JH, Tang C, Fu MW, Zhan YR (2014) Effect of discharge voltage on the deformation of Ti grade 1 rivet in electromagnetic riveting. Mater Sci Eng A 591:26–32
13. Zhang QL, Cao ZQ, Qin LG, Chen YQ (2013) Numerical simulation of electromagnetic riveting titanium alloy. Rare Metal Mater Eng 42:1832–1837
14. Feng DG, Cao ZQ (2012) Quality comparing analysis of electromagnetic riveting and pneumatic riveting. Forg StampTechnol 6: 62–65
15. Zhang X, Yu HP, Li J, Li CF (2015) Microstructure investigation and mechanical property analysis in electromagnetic riveting. Int J Adv Manuf Technol 78:613–623
16. Min JY, Li YQ, Li J, Li JJ, Carlson BE, Lin JP (2015) Friction stir blind riveting of carbon fiber-reinforced polymer composite and aluminum alloy sheets. Int J Adv Manuf Technol 76:1403–1410
17. Zhang X, Yu HP, Li CF (2014) Multi-filed coupling numerical simulation and experimental investigation in electromagnetic riveting. Int J Adv Manuf Technol 73:1751–1763